ARTICLES
PUBLISHED ONLINE: 28 MARCH 2010 | DOI: 10.1038/NCHEM.591
nature chemistry

Charge-transfer-induced structural rearrangements at both sides of organic/metal interfaces

Tzu-Chun Tseng[1], Christian Urban[2], Yang Wang[3], Roberto Otero[2,4]*, Steven L. Tait[1,5]*, Manuel Alcamí[3], David Écija[2], Marta Trelka[2], José María Gallego[6], Nian Lin[1,7], Mitsuharu Konuma[1], Ulrich Starke[1], Alexei Nefedov[8], Alexander Langner[1], Christof Wöll[9], María Ángeles Herranz[10], Fernando Martín[3], Nazario Martín[4,10], Klaus Kern[1,11] and Rodolfo Miranda[2,4]

Organic/metal interfaces control the performance of many optoelectronic organic devices, including organic light-emitting diodes or field-effect transistors. Using scanning tunnelling microscopy, low-energy electron diffraction, X-ray photoemission spectroscopy, near-edge X-ray absorption fine structure spectroscopy and density functional theory calculations, we show that electron transfer at the interface between a metal surface and the organic electron acceptor tetracyano-*p*-quinodimethane leads to substantial structural rearrangements on both the organic and metallic sides of the interface. These structural modifications mediate new intermolecular interactions through the creation of stress fields that could not have been predicted on the basis of gas-phase neutral tetracyano-*p*-quinodimethane conformation.

Organic heterostructures based on blends of molecules with electron-accepting (large electron-affinity) and electron-donating (small ionization potential) character display interesting electrical and optical properties with promising technological applications[1]. For example, they show the electroluminescence necessary for organic light-emission diodes (OLEDs) or field-effect transistors (OFETs)[2,3], a photovoltaic response suitable for solar cell devices[4,5] and one-dimensional conduction for low-molecular-weight metallic films[6], while their strong acceptors or donors can form the basis for metal–organic magnets[7–9]. These blends of molecules are deposited onto or placed in contact with metallic layers, and their performance thus depends crucially on both purely electronic factors (such as alignment of energy levels, electronic localization[10,11] or electronic coupling between molecular orbitals and metal electronic states) and morphology (such as molecular nanostructure[12] and crystalline perfection[13]). Interfaces between organic species having either a donor or acceptor character and metal surfaces are, thus, of paramount importance for the performance of the devices described above. This observation has motivated great interest in understanding the electronic structure of organic/metal interfaces[14] and, in particular, the alignment of the energy levels at the interface related to the charge transfer between the organic donor or acceptor species and the metallic surface[15–19]. Charge transfer, however, not only leads to modifications in the alignment of energy levels, but is usually also related to structural transformations in both donating and accepting species[20,21]. Unfortunately, the role of the substrate in supramolecular organization at surfaces is often overlooked or neglected and is not well understood.

We describe here experiments and theoretical simulations that unequivocally demonstrate that, for strong charge-transfer systems, both the molecules and the substrate undergo strong structural rearrangements that determine molecular ordering. Such charge-transfer-induced structural rearrangements at both sides of the organic/metal interface might have significant effects on the subsequent growth and structure of the organic film and, therefore, on device performance. In the following we describe the effect that charge transfer across the interface between a Cu(100) crystal and the organic acceptor tetracyano-*p*-quinodimethane (TCNQ) has on the conformation of adsorbed TCNQ molecules, on the structural rearrangement of the surface underneath the adsorbate and, therefore, on the self-assembly of TCNQ on Cu(100).

TCNQ is one of the strongest organic electron acceptors and has long been regarded as a prime candidate for organic/inorganic charge-transfer compounds[22]. The interface between TCNQ and copper can thus be considered a model system for the interfaces between the strong organic acceptors usually involved in OLEDs or organic solar cells and the metallic contacts. A combination of scanning tunnelling microscopy (STM), low-energy electron diffraction (LEED), X-ray photoelectron spectroscopy (XPS), near-edge X-ray absorption fine structure spectroscopy (NEXAFS) and density functional theory (DFT) calculations shows that the donation of about one electron from the substrate to the TCNQ molecules leads to a molecular conformation very similar to the well-documented structure of the anion or the dianion in solution. The conformation of the anionic molecule allows strong bonding between the nitrogen lone pairs and the copper atoms at the surface, so strong indeed that the surface atoms bonded to the cyano groups are significantly lifted from their usual positions at the surface. Finally, the stress field associated with the local reconstruction mediates new adsorbate–adsorbate interactions,

[1]Max Planck Institute for Solid State Research, D-70569 Stuttgart, Germany, [2]Departamento de Física de la Materia Condensada, Universidad Autónoma de Madrid, Cantoblanco, 28049 Madrid, Spain, [3]Departamento de Química, Universidad Autónoma de Madrid, 28049 Madrid, Spain, [4]Instituto Madrileño de Estudios Avanzados en Nanociencia (IMDEA-Nanociencia), Cantoblanco, 28049 Madrid, Spain, [5]Department of Chemistry, Indiana University, Bloomington, Indiana 47405, USA, [6]Instituto de Ciencia de Materiales de Madrid - CSIC, Cantoblanco, 28049 Madrid, Spain, [7]Department of Physics, The Hong Kong University of Science and Technology, Clear Water Bay, Kowloon, Hong Kong, China, [8]Lehrstuhl für Physikalische Chemie, Ruhr-Universität Bochum, 44780 Bochum, Germany, [9]Institute of Functional Interfaces, Karlsruhe Institute of Technology (KIT), 76012 Karlsruhe, Germany, [10]Departamento de Química Orgánica, Universidad Complutense de Madrid, 28040 Madrid, Spain, [11]Institut de Physique de la Matière Condensée, Ecole Polytechnique Fédérale de Lausanne, CH-1015 Lausanne, Switzerland. *e-mail: roberto.otero@uam.es; tait@indiana.edu

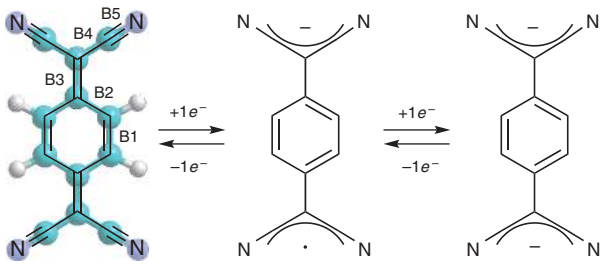

Figure 1 | Chemical structure of TCNQ, $TCNQ^{\bullet -}$ and $TCNQ^{2-}$. In the neutral form the bond B3 in TCNQ is double and the central ring is not aromatic. The uptake of at least one electron, however, aromatizes the central ring, changing B3 from double to single and enhancing the conformational freedom of the molecule[24].

and thereby results in a peculiar anisotropic growth for the self-assembled two-dimensional islands that could not have been predicted on the basis of the gas-phase conformation of TCNQ. Although some of these processes (charge transfer, adsorbate conformational changes, adsorbate-induced reconstructions) had been suggested to have a role in the self-assembly of organic acceptors on solid surfaces[20,21,23], the causal link among these processes could only be revealed by a powerful combination of complementary experimental and theoretical tools such as the one presented in this work. Moreover, such a combination of techniques enables us to quantify the strength of this effect rather than just suggesting its likelihood. This effect illustrates the important consequences that strong electronic interactions at the interface between organic donors or acceptors and metallic electrodes might have on the crystal structure of organic thin films contacted to them, and calls for further growth studies to characterize organic/metal interfaces for technological applications.

The chemical structure of TCNQ is outlined in Fig. 1. The main features that determine TCNQ acceptor functionality are the four peripheral cyano groups and the central hexagonal ring. In its neutral form the hexagonal ring is not aromatic and the molecular conformation is very rigid owing to the alternation of multiple and single bonds (*p*-quinoid character). The uptake of one electron, however, aromatizes the central hexagon ring (Fig. 1), which can only take place by changing bond B3 from double to single. The extra electron is thus accommodated in one of the peripheral nitrogen atoms, so that one of the molecular ends remains radical in character, whereas the other end loses the radicaloid character by accumulating one extra electron. Bond conjugation at the dicyanomethylene ends, however, remains, so that both the extra electron and the radical character are delocalized at each dicyanomethylene group.

The dianion form of TCNQ is also well known: in this case the second electron is accommodated at the radicaloid dicyanomethylene end. In the anionic and dianionic forms, bond conjugation is restricted to the central ring and to the dicyanomethylene groups: the terminal carbon of bond B3 now has a higher sp^3 character and, consequently, the cyano groups are able to bend. The conformational freedom of $TCNQ^{\bullet -}$ and $TCNQ^{2-}$ is thus much larger than that of neutral TCNQ[24]. Charge transfer can therefore be expected to influence strongly the structure of the TCNQ/metal interface.

Results

TCNQ adsorbs initially along the electron-rich step edges on Cu(100), as on Cu(111)[25], but with the molecular long axis perpendicular to the step. Further growth proceeds from the steps in the shape of two-dimensional compact islands, with a well-defined rectangular shape (see Fig. 2), the longer side of which is perpendicular

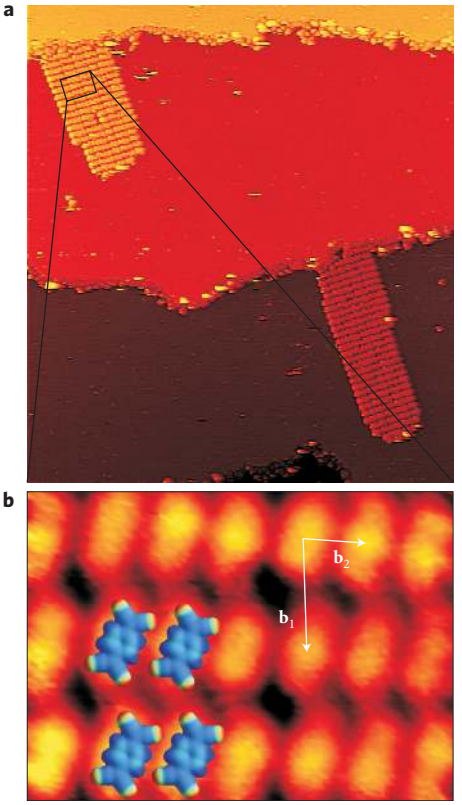

Figure 2 | Elongated self-assembled islands of TCNQ on Cu(100). **a**, Representative STM image (80×80 nm^2) showing the elongated TCNQ islands on Cu(100). The sample was prepared by thermally evaporating TCNQ (crucible temperature of ~340 K) onto the Cu(100) crystal held at room temperature. The STM image was recorded at room temperature, because investigation at lower temperatures did not lead to any significant changes in sample morphology. **b**, Details of the molecular arrangement. Constant charge density isosurfaces for TCNQ molecules, calculated in the gas phase, have been superimposed on the STM image. The projection of the electrostatic potential over the surface has been colour-coded onto it, in such a way that the red areas correspond to areas in which the electrostatic potential is negative and the blue-coded areas represent positive potential.

to the step. TCNQ molecules, both at step edges and in rectangular islands, appear as ellipsoids, with an apparent size of 11Å × 6 Å and an apparent height of $\sim 1.3 \pm 0.3$ Å, which is consistent with an adsorption geometry in which the average molecular plane is parallel to the surface.

Figure 3 shows a close-up STM image of a TCNQ island and the LEED pattern for a TCNQ coverage close to one monolayer (ML) deposited on Cu(100) (a monolayer is defined as the amount of material that would cover the whole surface with a one-layer-thick molecular layer, assuming that the in-plane ordered structure is the one described in Figs 2 and 3). Clearly visible in the STM images is the existence of a quasi-periodic array of one-dimensional dislocation lines in the molecular overlayer every three or four molecular rows. In the dislocation-free regions, our measurements are compatible with a structure commensurate with the Cu(100) lattice, with unit cell vectors given by $\mathbf{b}_1 = 4\mathbf{a}_1 + 3\mathbf{a}_2$ and $\mathbf{b}_2 = -2\mathbf{a}_1 + 2\mathbf{a}_2$, with $\mathbf{a}_1$ and $\mathbf{a}_2$ being the unit cell vectors of the underlying Cu(100) substrate. Across the dislocation lines (which run parallel to the $\mathbf{b}_1$ direction), the whole molecular row is shifted by one Cu(100) lattice parameter and the vector linking equivalent molecules across the dislocation line can be written as $\mathbf{b}_2 = -2\mathbf{a}_1 + 3\mathbf{a}_2$. We have checked that the combination of these two structures (also taking into account the existence of four

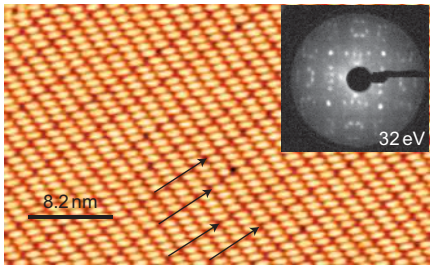

Figure 3 | Highly ordered self-assembled monolayer of TCNQ on Cu(100). STM close-up image of TCNQ monolayer island structure on Cu(100). Some dislocation lines (described in the text) are marked by arrows. Inset: LEED pattern recorded at 32 eV. The unit cell dimensions and symmetry as determined by STM are in good agreement with those obtained by LEED (see text).

different domains) yields a LEED pattern in complete agreement with the experimental one.

As mentioned above, the TCNQ islands grow in a manner elongated along the $\mathbf{b}_1$ direction. Statistical analysis of the self-assembled TCNQ island morphologies shows that the aspect ratio, that is, the ratio between the length of the long side of the island and the length of the short side of the island, is 4.3 ± 1.5, corresponding to $\sim 2.4 \pm 0.8$ times more molecules along $\mathbf{b}_1$ than $\mathbf{b}_2$. We conclude that the interaction linking the molecules along $\mathbf{b}_1$ must be larger than the interaction that holds the molecules together along $\mathbf{b}_2$. This is a rather surprising conclusion if we consider the charge distribution of neighbouring TCNQ molecules placed at the experimentally determined distances.

Figure 2b presents electrostatic potential maps evaluated at a surface of constant electronic density, with a colour code that indicates the sign of the potential (red for negative and blue for positive); these have been superimposed on our molecularly resolved STM images. The isosurfaces have been calculated for neutral TCNQ molecules in the gas-phase conformation. Red-coded areas represent negatively charged areas, and blue-coded areas represent areas with a positive partial charge. The interaction along $\mathbf{b}_2$ can, thus, be ascribed to electrostatic interaction between the negatively charged cyano groups and hydrogen atoms of the central ring. This is the main bonding motif for self-assembled monolayers of TCNQ on the Au(111) surface[26]. On the other hand, the origin of the interaction along $\mathbf{b}_1$ remains unclear with this approximation, as it seems to bring together two negatively charged cyano groups.

XPS reveals the charge-transfer effects of TCNQ/Cu(100) by comparing the core level shifts with neutral TCNQ (see Fig. 4). The nitrogen 1*s* core level spectrum for neutral TCNQ shows a single peak at 399.6 eV, and a satellite or 'shake-up' structure, characteristic of XPS peaks for semiconductors and insulators, is found at 2.4 eV higher binding energy. The presence of the metal suppresses the shake-up feature for TCNQ/Cu(100), and the nitrogen 1*s* level is shifted towards lower binding energy (398.7 eV), indicating charge transfer from the copper substrate into the TCNQ molecule (a similar trend is found on all the components found for the carbon 1*s* peak, see Supplementary Fig. S1). This charge transfer is probably responsible for the observed increase of the work function by 0.6 eV on completion of the monolayer in the related fluorinated TCNQ adsorbed on Cu(111)[20]. With the structure that we obtain by STM and LEED, this charge transfer would amount to an induced dipole moment of 1.6 D per molecule. The central, quinoid ring of adsorbed TCNQ becomes aromatic on charge transfer. As discussed above, TCNQ gains some conformational freedom on charge transfer, which might explain the seemingly unfavourable interaction shown in the inset of Fig. 2 (see the discussion below).

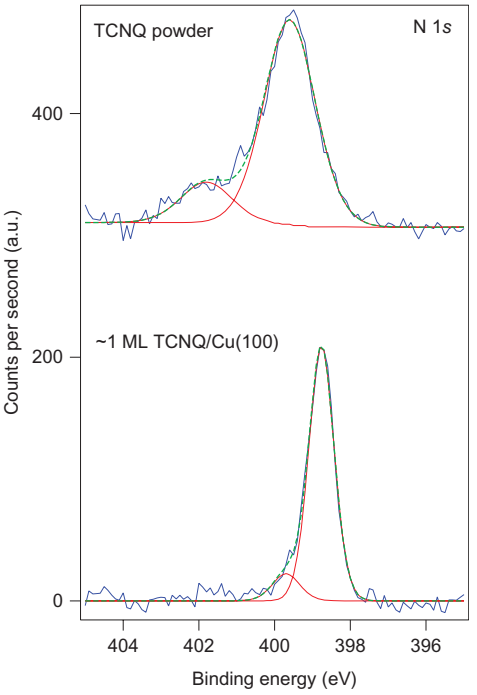

Figure 4 | Charge transfer in a self-assembled monolayer of TCNQ on Cu(100). XPS spectra of nitrogen 1s core levels for TCNQ/Cu(100) and a bulk sample (powder) of TCNQ. The spectra show raw experimental data (blue), the fit to the experimental data (green) and the decomposition of the fit into their individual components (red). In each spectrum, a high-energy shoulder is visible, this being the molecular 'shake-up' peak (see main text for further details). On adsorption at the Cu(100) surface, the nitrogen 1s core level of the TCNQ shifts by 0.9 eV to a lower binding energy, indicative of electron transfer from the copper substrate to the TCNQ.

To understand the conformation and bonding geometry of TCNQ on the Cu(100) surface, an angle-resolved NEXAFS study was performed at the Berliner Elektronen-Speicherring Gesellschaft für Synchrotronstrahlung (BESSY). The spectra, shown in Fig. 5, were normalized and fitted according to standard procedures for NEXAFS analysis[27,28]. In Fig. 5a, the nitrogen 1*s* NEXAFS spectra of TCNQ powder and 1 ML TCNQ/Cu(100) are shown. In comparison with previous works, peaks 1 and 3 are attributed to the central ring of TCNQ, whereas peak 2 is assigned to the CN group[29–31]. In agreement with our XPS results, we interpret the absence of resonance 1 on adsorption as the result of charge-transfer populating the LUMO orbital and aromatizing the central quinoid ring. Resonance 2 contains the two orthogonal π^*-orbitals of the CN group, which lie close in energy for neutral molecules. However, on adsorption, the strong interaction of CN to the Cu(100) substrate leads to the splitting of such contributions, and separates peak 2 into peaks $2'_a$ and $2'_b$ in the nitrogen 1*s* NEXAFS spectra. The bonding angle of TCNQ can be determined by analysing the intensity dependence of resonances with incident X-ray direction as shown in Fig. 5b. The direction of the incident beam is characterized by the angle ϕ between the beam and the surface normal. This angular dependence is analysed by fitting with a formula that contains the bonding angle (angle between the bond and the surface) of TCNQ (Supplementary Fig. S2), and thus one obtains 19.7° and 10.0° from peaks $2'_a$ and $2'_b$, respectively. Together with the carbon 1*s* analysis, shown in the Supplementary Information, we can conclude that TCNQ lies on Cu(100), with the central ring flat adsorbed and the CN group tilted with a bonding angle of 10.0–19.7°. This bent conformation of TCNQ is supported by DFT calculations, which we will discuss in the following.

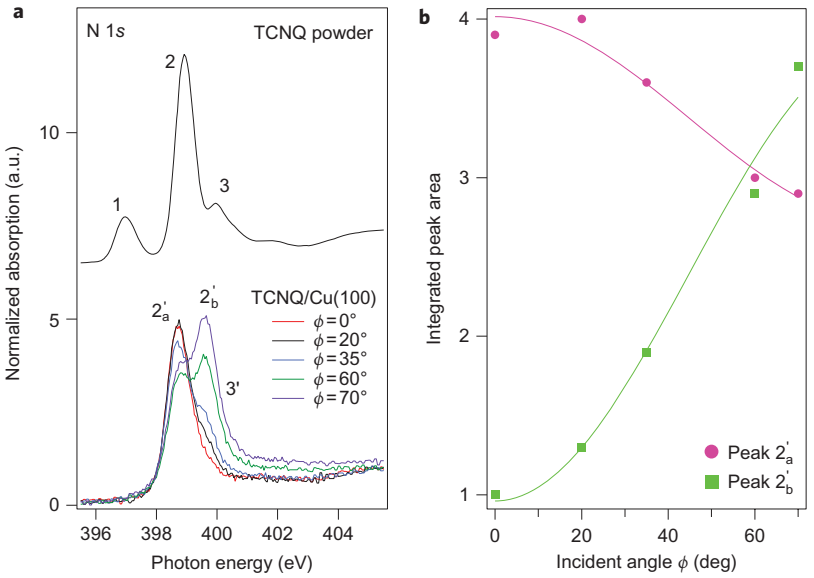

Figure 5 | NEXAFS measurements of TCNQ / Cu(100). a, NEXAFS spectra for TCNQ powder (top), exhibiting three principal peaks. The bottom spectra are for a TCNQ monolayer on Cu(100) at various incident beam angles (ϕ). The absence of peak 1 is an indication of charge transfer from copper to TCNQ, as discussed in the text. **b**, Fits of the peak intensity versus beam angle for peaks $2'_a$ and $2'_b$. Best fits to these trends indicate a tilting of the cyano groups towards the surface on adsorption by 10.0–19.7°.

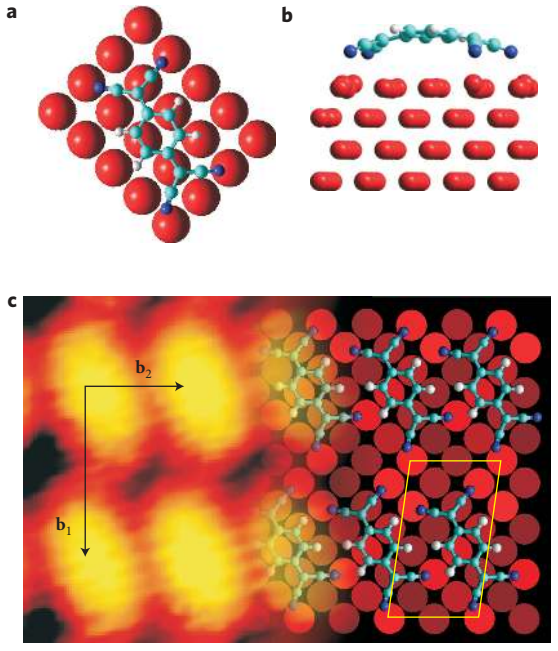

Figure 6 | Structural rearrangements at both sides of the TCNQ/Cu(100) interface from DFT calculations. a,**b**, Top (**a**) and side (**b**) views of the calculated relaxed conformation for a single TCNQ molecule adsorbed on Cu(100) (where light blue corresponds to carbon atoms, dark blue corresponds to nitrogen atoms, red corresponds to the copper atoms of the substrate and white corresponds to hydrogen atoms). Bending of the B3 bond and surface reconstruction are clearly observed. **c**, Top view of the calculated relaxed conformation for the self-assembled TCNQ monolayer. Different shades of red of the copper atoms represent different distances between the copper atom and the unperturbed, unreconstructed equilibrium position (the brightest red shade corresponds to copper atoms separated by 0.22 Å above their equilibrium positions, whereas the darkest shade corresponds to copper atoms placed 0.16 Å below the equilibrium position). Reconstructed atoms act as a glue to link molecular rows along $\mathbf{b}_1$.

To shed light on the interaction that holds the islands together along the $\mathbf{b}_1$ direction, we carried out DFT calculations for both isolated molecules adsorbed on Cu(100) and the complete overlayer (in this case with the experimentally obtained unit cell vectors). The optimized geometry for the adsorbed monomeric TCNQ is shown in Fig. 6a,b. This geometry corresponds to the minimum of all the configurations explored for the single molecule adsorbed on Cu(100). The calculated binding energy is 2.23 eV, indicating a rather strong chemisorption. The calculated binding energy for the complete overlayer is slightly larger, 2.35 eV molecule^{-1}, indicating further stabilization of the system owing to the particular organization of the overlayer. The orientation of the molecule with respect to the high-symmetry directions of the Cu(100) surface agrees well with the one observed in the STM images (as shown in Fig. 6c), and seems to be fixed by the drive of the cyano groups to point towards the top positions of the Cu(100) surface. Interestingly, the conformation of the TCNQ molecule is not planar, but the B3 bond is bent so that the cyano groups point towards the surface. Such a bending of the B3 bond is energetically very costly unless the conjugation of double and single bonds associated with the neutral form of TCNQ is removed by the uptake of at least one electron from the surface. A theoretical estimation based on a Bader analysis of the charge density yields a transfer from the Cu(100) surface to the TCNQ adsorbate of 1.5 e^- per TCNQ, in qualitative agreement with the XPS results shown in Fig. 3. Such a bent geometry has already been described for the related F4-TCNQ species adsorbed on a Cu(111) surface, and was also attributed to charge transfer from the surface[20]. In contrast, adsorption of TCNQ on Au(111), a surface for which the charge transfer is expected to be much lower owing to its larger work function and overall reduced reactivity, does not result in a bent conformation of the adsorbate[32].

Discussion

The bending of the dicyano moieties towards the surface enables a rather strong chemical interaction between the lone pairs of the nitrogen atoms and the d_z orbitals of copper. Such strong interactions lead to a high adsorption energy and, more importantly, to a rearrangement of the coppper surface atoms bonded to the cyano groups. As can be seen in Fig. 6b, these copper atoms are

lifted from their equilibrium positions by about 0.3 Å. A similar surface reconstruction has been theoretically obtained for the adsorption of the related tetracyanoethylene molecule on Cu(100)[21], also a strong organic acceptor. The rearrangement of these copper atoms creates a stress field in such a way that the energy cost to lift a second atom out of its unperturbed equilibrium position is significantly reduced for the immediate neighbours of the already reconstructed copper atom bonded to the cyano group.

Figure 6c shows a top view of the calculated relaxed geometry for a self-assembled TCNQ overlayer on Cu(100). The out-of-plane position of the copper atoms has been colour-coded in different shades of red, in such a way that lighter shades of red indicate atoms protruding farther out from the surface. A close inspection of the spatial distribution of such reconstructed atoms reveals that they are mainly located at the bonding positions with the cyano groups in the TCNQ molecules. The stress field around the reconstructed atoms makes it energetically favourable for copper atoms attached to cyano groups of different molecules to be in close proximity, and therefore has a profound effect on the self-ordering of TCNQ islands.

In the present case, reconstructed copper atoms are tightly grouped along the $\mathbf{b}_1$ direction of the TCNQ layer. We can thus understand the significant attractive interaction along $\mathbf{b}_1$, which leads to high-aspect-ratio rectangular islands, as a result of a surface-strain mediated interaction enabled by the conformational freedom that TCNQ gains owing to charge transfer from the surface. Although substrate-mediated elastic interactions have been invoked before to explain the ordering of several nanostructures on solid surfaces, for example copper–oxygen islands formed on partial oxidation of the Cu(110) surface, the distance range in which they have a significant role is usually one order of magnitude larger than the one described here[33–36].

The results shown here exemplify the fundamental role that charge-transfer processes across metal/organic interfaces have on molecular self-assembly and subsequent crystal growth. Such charge transfers modify energy level alignment, but they also affect molecular conformation and, thereby, adsorbate self-assembly. For example, they are usually related to the existence of strong bonding between surface and adsorbate, and in such situations the static-surface approximation is no longer applicable: substrate reconstruction and surface-mediated interactions must be explicitly taken into account, and gas-phase expectations based on intermolecular interactions are not likely to work. These arguments prompt further studies to properly address the relation between electronic interactions and geometrical structure in organic/metal interfaces, which should contribute significantly to the development of high-performance optoelectronic devices. For example, comparison with molecules containing cyano groups but not having such a strong accepting character, or with strong organic acceptors not containing cyano groups, will further clarify the interplay between charge transfer and chemical bonding across the interface.

Methods

To study the effect of charge transfer on the structure of the interfaces between organic acceptors and metal electrodes, we have grown submonolayer-thick TCNQ films on Cu(100) surfaces. Film growth and STM, XPS and LEED investigations were carried out in ultrahigh-vacuum (UHV) conditions, with a base pressure of $<2 \times 10^{-10}$ torr, to allow precise control of surface composition[37]. Atomically flat, crystalline Cu(100) surfaces were prepared by standard sputter/anneal procedures (sputter with 1 kV Ar^+ ions for 15 min followed by annealing to 800 K for another 15 min), resulting in large terraces (~200 nm wide) separated by monoatomic steps. The molecules were deposited from a low-temperature Knudsen cell, heated at 350 K, onto the clean Cu(100) substrate, which was held at room temperature. Two different STMs were used to image the surface, in both cases at room and low (~100 K) temperature, and the images show no significant difference. Tunnelling conditions were chosen so as not to disturb individual molecules ($V_{bias} \approx 1$–2 V, $I_t \approx 100$–500 pA). The XPS spectra were recorded in a separate chamber using aluminium K_α X-rays of 1,486.6 eV. One of the STM chambers and the XPS chamber were equipped with LEED facilities. The diffraction patterns obtained were identical.

DFT calculations were performed using VASP code with the PerdewWang (PW91)[38] functional. The projector augmented wave (PAW) method[39,40] was used to describe the ionic cores. The MonkhorstPack scheme with a k-point mesh of $1 \times 1 \times 1$ k-points was used. A Methfessel-Paxton smearing[41] of 0.4 eV was applied. The energy cut-off in the plane-wave expansion was set to 400 eV. Four layers of copper were used, with the bottom two held fixed and the top two (plus all the atoms in the molecules) allowed to relax. For the isolated TCNQ adsorbed on the surface, a 7×5 surface unit cell was used to prevent intermolecular interactions. For self-assembled isolated TCNQ adsorbed on the surface, the unit cell shown in Fig. 6c was used. Dipole correction was applied during all the computations. The charge transfer was evaluated based on Baders topological analysis of the charge density obtained by VASP calculation (http://theory.cm.utexas.edu/vtsttools/bader/).

Received 16 July 2009; accepted 9 February 2010; published online 28 March 2010

References

1. Forrest, S. R. The path to ubiquitous and low-cost organic electronic appliances on plastic. *Nature* **428,** 911–918 (2004).
2. Moons, E. Conjugated polymer blends: linking film morphology to performance of light emitting diodes and photodiodes. *J. Phys. Condens. Matter.* **14,** 12235–12260 (2002).
3. Cicoira, F. & Santato, C. Organic light emitting field effect transistors: advances and perspectives. *Adv. Funct. Mater.* **17,** 3421–3434 (2007).
4. Blom, P. W. M., Mihailetchi, V. D., Koster, L. J. A. & Markov, D. E. Device physics of polymer:fullerene bulk heterojunction solar cells. *Adv. Mater.* **19,** 1551–1566 (2007).
5. Brabec, C. J., Sariciftci, N. S. & Hummelen, J. C. Plastic solar cells. *Adv. Funct. Mater.* **11,** 15–26 (2001).
6. Jérome, D. Organic conductors: from charge density wave TTF–TCNQ to superconducting $(TMTSF)_2PF_6$. *Chem. Rev.* **104,** 5565–5591 (2004).
7. Manriquez, J. M., Yee, G. T., Scott McLean, R., Epstein, A. J. & Miller, J. S. A room-temperature molecular/organic-based magnet. *Science* **252,** 1415–1417 (1991).
8. Jain, R. *et al.* High-temperature metallorganic magnets. *Nature* **445,** 291–294 (2007).
9. Gambardella, P. *et al.* Supramolecular control of the magnetic anisotropy in two-dimensional high-spin Fe arrays at a metal interface. *Nature Mater.* **104,** 189–193 (2009).
10. Zhu, X.-Y. Electronic structure and electron dynamics at molecule–metal interfaces: implications for molecule based electronics. *Surf. Sci. Rep.* **56,** 1–83 (2004).
11. Lindstrom, C. D. & Zhu, X.-Y. Photoinduced electron transfer at molecule–metal interfaces. *Chem. Rev.* **106,** 4281–4300 (2006).
12. Otero, R. *et al.* An organic donor/acceptor lateral superlattice at the nanoscale. *Nano Lett.* **7,** 2602–2607 (2007).
13. Barth, J. V., Constantini, G. & Kern, K. Engineering atomic and molecular nanostructures at surfaces. *Nature* **437,** 671–679 (2005).
14. Wang, L., Chen, W. & Thye Shen Wee, A. Charge-transfer across the molecule/metal interface using the core hole clock technique. *Surf. Sci. Rep.* **63,** 465–386 (2008).
15. Ishii, H., Sugiyama, K., Ito, E. & Seki, K. Energy level alignment and interfacial electronic structures at organic/metal and organic/organic interfaces. *Adv. Mater.* **11,** 605–625 (1999).
16. Crispin, X. *et al.* Characterization of the interface dipole at organic/metal interfaces. *J. Am. Chem. Soc.* **124,** 8131–8141 (2002).
17. Koch, N., Duhm, S., Rabe, J. P., Vollmer, A. & Johnson, R. L. Optimized hole injection with strong electron acceptors at organic–metal interfaces. *Phys. Rev. Lett.* **95,** 237601 (2005).
18. Witte, G., Lukas, S., Bagus, P. S. & Wöll, C. Vacuum level alignment at organic/metal junctions: 'cushion' effect and the interface dipole. *Appl. Phys. Lett.* **87,** 263502 (2005).
19. Braun, S. & Salaneck, W. R. Fermi level pinning at interfaces with tetrafluorotetracyanoquinodimethane (F_4-TCNQ): the role of integer charge transfer states. *Chem. Phys. Lett.* **438,** 259–262 (2007).
20. Romaner, L. *et al.* Impact of bidirectional charge transfer and molecular distortions on the electronic structure of a metal–organic interface. *Phys. Rev. Lett.* **99,** 256801 (2007).
21. Bedwani, S., Wegner, D., Crommie, M. F. & Rochefort, A. Strongly reshaped organic–metal interfaces: tetracyanoethylene on Cu(100). *Phys. Rev. Lett.* **101,** 216105 (2008).
22. Torrance, J. B. The difference between metallic and insulating salts of tetracyanoquinodimethane (TCNQ): how to design an organic metal. *Acc. Chem. Res.* **12,** 79–86 (1979).
23. Wegner, D. *et al.* Single-molecule charge transfer and bonding at an organic/inorganic interface: tetracyanoethylene on noble metals. *Nano Lett.* **8,** 131–135 (2008).
24. Milián, B., Pou-Amérigo, R., Viruela, R. & Ortí, E. A theoretical study of neutral and reduced tetracyano-*p*-quinodimethane (TCNQ). *J. Mol. Struct.* **709,** 97–102 (2004).

25. Kamna, M. M., Graham, T. M., Love, J. C. & Weiss, P. S. Strong electronic perturbation of the Cu(111) surface by 7,7',8,8'-tetracyanoquinonedimethane. *Surf. Sci.* **419,** 12–23 (1998).
26. Fernández-Torrente, I., Franke, K. J. & Pascual, J. I. Structure and electronic configuration of tetracyanoquinodimethane layers on a Au(111) surface. *Int. J. Mass Spectrosc.* **277,** 269–273 (2008).
27. Stöhr, J. & Outka, D. A. Determination of molecular orientations on surfaces from the angular dependence of near-edge X-ray-absorption fine-structure spectra. *Phys. Rev. B* **36,** 7891–1905 (1987).
28. Stöhr, J. *NEXAFS Spectroscopy* (Spinger-Verlag, 2003).
29. Bässler, M. *et al.* Near edge X-ray absorption fine structure resonances of quinoide molecules. *Langmuir* **16,** 6674–6681 (2000).
30. Sing, M. *et al.* Structural versus electronic origin of renormalized band widths in TTF–TCNQ: an angular dependent NEXAFS study. *Phys. Rev. B* **76,** 245119 (2007).
31. Fraxedas, J. *et al.* Characterization of the unoccupied and partially occupied states of TTF–TCNQ by XANES and first-principles calculations. *Phys. Rev. B* **68,** 195115 (2003).
32. González Lakunza, N. Study of the geometry and electronic structure of self-assembled monolayers on the Au(111) surface. PhD thesis, Universidad del Pais Vasco (2009).
33. Kern, K. *et al.* Long-range spatial self-organization in the adsorbate-induced restructuring of surfaces: Cu(110)–(2×1)O. *Phys. Rev. Lett.* **67,** 855–858 (1991).
34. Zeppenfeld, P. *et al.* Size relation for surface systems with long-range interactions. *Phys. Rev. Lett.* **72,** 2737–2740 (1994).
35. Prevot, G. *et al.* Elastic origin of the O/Cu(110) self-ordering evidenced by GIXD. *Surf. Sci.* **549,** 52–56 (2004).
36. Tait, S. L. *et al.* One-dimensional self-assembled molecular chains on Cu(100): interplay between surface-assisted coordination chemistry and substrate commensurability. *J. Phys. Chem. C* **111,** 10982–10987 (2007).
37. Tait, S. L. Function follows form: exploring 2D supramolecular assembly at surfaces. *ACS Nano* **2,** 617–621 (2008).
38. Perdew, J. P. & Wang, Y. Accurate and simple analytic representation of the electron–gas correlation energy. *Phys. Rev. B* **45,** 13244–13249 (1992).
39. Blöchl, P. E. Projector augmented-wave method. *Phys. Rev. B* **50,** 17953–17979 (1994).
40. Kresse, G. & Joubert, D. From ultrasoft pseudopotentials to the projector augmented-wave method. *Phys. Rev. B* **59,** 1758–1775 (1999).
41. Methfessel, A. & Paxton, A. T. High-precision sampling for Brillouin-zone integration in metals. *Phys. Rev. B* **40,** 3616–3621 (1989).

Acknowledgements

Studies at MPI Stuttgart were supported by the European Science Foundation (ESF) EUROCORES-SONS2 programme FunSMARTs II. Work in Madrid was financed by the Spanish MICINN (projects FIS2007-61114, FIS2007-60064, NAN2004-08881-C02-01, CTQ2006-08558 and Consolider CSD2007-00010), the Comunidad de Madrid (projects S-0505-MAT-0194 and S2009/MAT-1726) and the European Union ('MONET' project, MEST-CT-2005-020908). R.O. thanks the MEC for salary support through the Ramón & Cajal programme. All the computations were performed at Mare Nostrum Barcelona Supercomputer Center and Centro de Computación Científica de la UAM.

Author contributions

STM experiments were carried out by T.-C.T., C.U. and M.T. T.-C.T. and C.U. contributed equally to this work. T.-C.T., C.U. and D.E. were involved in STM data analysis. Y.W., M.A. and F.M. carried out the DFT calculations shown in this paper. T.-C.T., S. L.T., M.K. and U.S. performed the XPS and LEED measurements and analysis, and T.-C.T., A.L., S.L.T. and A.N. performed the NEXAFS experiments and analysis, supervised by C.W. The molecules were provided by M.A.H. and N.M. and they supervised the chemical discussions. R.O., J.M.G. and S.L.T. wrote the paper and coordinated all the experimental work. Experiments were planned and designed by R.O., J.M.G., S.L.T., U.S. and N.L. under the supervision of K.K. and R.M.

Additional information

The authors declare no competing financial interests. Supplementary information accompanies this paper at www.nature.com/naturechemistry. Reprints and permission information is available online at http://npg.nature.com/reprintsandpermissions/. Correspondence and requests for materials should be addressed to R.O. and S.L.T.